



Semnan University



# Analyzing the Effect of using Electromagnetic Metamaterials in the Production of Plane Spiral Orbital Angular Momentum Waves (PSOAM)

Roghieh Karimzadeh Bae<sup>1</sup> <sup>\*</sup>, Reza Darvishi<sup>2</sup>

**Abstract--** The utilization of orbital angular momentum (OAM) presents an effective approach that enables the simultaneous use of multiple channels on a single frequency. Compared with conventional OAM carrier waves—whose three-dimensional radiation pattern resembles a cone with a hollow region at its center—the planar-spiral orbital angular momentum (PSOAM) carrier propagates transversely, making it more suitable for various practical applications. For the first time, the generation of PSOAM waves using a uniform circular array of microstrip antennas based on electromagnetic metamaterials has resulted in a phase pattern distinct from the conventional OAM theory. This study demonstrates that incorporating metamaterials into the antenna array structure facilitates the generation of higher-order OAM modes with fewer elements than conventional antennas. Simulation results indicate that the proposed array achieves approximately a 27% reduction in the number of antenna elements. Furthermore, the introduced antenna exhibits a wide relative bandwidth of 1.93.

**Keywords—**Orbital angular momentum, planar spiral orbital angular momentum, circular array, electromagnetic metamaterials

## I. INTRODUCTION

Electromagnetic waves are the primary means of information transfer in modern telecommunication systems. Beyond merely transporting energy, these waves also convey various physical properties, including angular momentum [1]. Angular momentum consists of two primary components: spin angular momentum (SAM) [2] and orbital angular momentum (OAM) [3]. While SAM is

associated with changes in the polarization state of electromagnetic waves, OAM corresponds to the azimuthal phase rotation along the wave propagation axis. The unique orthogonality of OAM modes allows their simultaneous use across multiple communication channels, substantially enhancing the capacity of telecommunication systems [1]. These properties have led to extensive applications in areas such as target detection and imaging [6]–[7], radar systems for rotating target identification [8], Doppler effect measurement [9], and quantum communication protocols [10].

Several techniques exist for generating millimeter-wave OAM beams in radio-frequency systems, including spiral phase plates [4] and uniform circular arrays (UCAs) [5]. Recently, antennas capable of producing OAM waves have garnered significant attention due to their potential to revolutionize high-capacity communication, advanced radar systems, satellite links, and quantum communications. These antennas are particularly valuable in frequency-constrained telecommunication environments, enabling concurrent transmission of multiple distinct OAM modes at a single carrier frequency [2].

However, conventional OAM antennas typically exhibit a three-dimensional conical radiation pattern with a central null, necessitating large-aperture receiving antennas for long-range communications. To overcome this limitation, plane spiral orbital angular momentum (PSOAM) antennas have been proposed [11]–[12]. By utilizing different OAM modes at a fixed frequency, PSOAM antennas effectively increase channel capacity. In uniform circular arrays, the maximum achievable OAM mode order is constrained by the number of array elements [13]. PSOAM antennas, featuring planar spiral radiation patterns, address radiation challenges by providing improved performance over various orientations and reducing beam divergence—a prevalent issue in conventional

<sup>1</sup>Satellite Communication Group, Faculty of Communications Technology, ICT Research Institute, Tehran, Iran.

<sup>\*</sup>Corresponding author:Email: [rkbaee@itrc.ac.ir](mailto:rkbaee@itrc.ac.ir)

<sup>2</sup>Imam Hossein University, Tehran, Iran.

### Cite this article as:

Karimzadeh Bae, R. and Darvishi, R., 2024. Analyzing the Effect of uUsing Electromagnetic Metamaterials in the Production of Plane Spiral Orbital Angular Momentum Waves (PSOAM). *Journal of Modeling & Simulation in Electrical & Electronics Engineering (MSEEE)*, 4(4), pp. 51-57.

<https://doi.org/10.22075/MSEEE.2025.38236.1217>

OAM designs [14]. Fig. 1 illustrates the radiation patterns of OAM and PSOAM antennas, demonstrating the omnidirectional coverage of PSOAM that mitigates the beam divergence inherent to traditional OAM systems.

Although employing multiple OAM modes at a fixed frequency enhances channel capacity, a major challenge in OAM antenna design is the dependency of producible mode order on the array size. Higher-order modes require an increased number of array elements, leading to larger, heavier, and more complex antenna structures. Consequently, minimizing the element count while achieving higher-order modes remains a key design objective [5]. In [15], despite employing a circular array based on electromagnetic metamaterials, no reduction in the number of array elements was achieved, and the generated phase pattern remained consistent with the conventional theory.

Motivated by the need to generate higher-order OAM modes in compact arrays, this study explores the use of metamaterial-inspired elements in PSOAM antenna design. This approach aims to enhance capacity without increasing the overall array size or element count. In addition to characterizing the properties of metamaterial-based PSOAM antennas, the paper proposes a novel method for realizing higher-order OAM modes within compact antenna configurations.

The remainder of the paper is organized as follows: Section II presents the theoretical framework governing angular momentum wave generation. Section III describes the design principles of metamaterial-based microstrip array antennas for PSOAM wave generation. Section IV analyzes simulation results obtained using CST Studio Suite, demonstrating that the proposed array achieves higher-order OAM modes beyond conventional array antenna limitations—representing a significant step toward high-capacity, wideband communication systems.

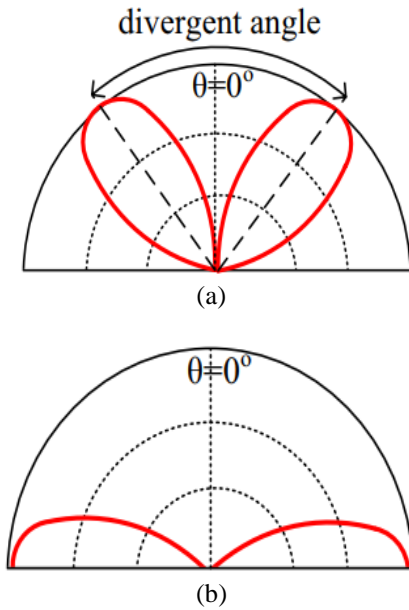


Fig. 1. Radiation pattern diagram of the E-plane for (a) OAM and (b) PSOAM configurations.

## II. MECHANISM OF PSOAM WAVE GENERATION BY A CONVENTIONAL CIRCULAR ANTENNA ARRAY

Fig. 2 illustrates the schematic of a circular array configuration along with the coordinates of its far-field radiation. The array elements are uniformly distributed along a circle. The point  $P(r, \theta, \phi)$  denotes the observation point in the antenna's far-field region, and  $\alpha_n$  represents the angle formed between the observation point  $P$ , the phase reference point (located at the center of the array), and the position of the  $n$ th element of the array.

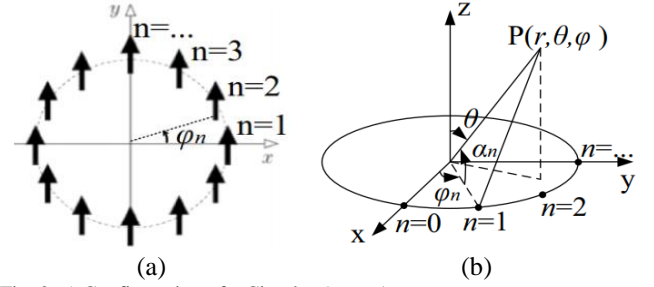


Fig. 2. a) Configuration of a Circular Array Antenna. b) Coordinate system for calculating the far-field electric field.

Equation (1) presents the array factor for the circular configuration shown in Fig. 2.

$$F(\theta, \phi) = \sum_{n=0}^{N-1} e^{j\Psi_n} e^{jka \cos \alpha_n} = \sum_{n=0}^{N-1} e^{jl\phi_n} e^{jka \sin \theta \cos(\phi - \phi_n)} \quad (1)$$

In this expression,  $a$  denotes the radius of the circular array, and  $k$  is the wavenumber. The angular position of the  $n$ -th element in the  $x$ - $y$  plane is defined as  $\phi_n = 2\pi n/N$ , where  $N$  is the total number of array elements and  $n = 0, 1, 2, \dots, N-1$ . The excitation (feeding) phase of each element is given by  $\Psi_n = l\phi_n$  and  $l$  represents the OAM mode number.  $k$  also represents the wave number.

For a sufficiently large number of elements ( $N$ ), (1) can be approximated by the following expression, based on the simplifications introduced in [16]:

$$F(\theta, \phi) = N j^l J_l(ka \sin \theta) e^{jl\phi} \quad (2)$$

In this expression,  $J_l(\cdot)$  denotes the Bessel function of the first kind of order  $l$ . As shown in (2), a uniform circular array (UCA) antenna is capable of generating electromagnetic vortex waves. Since the key distinction between PSOAM and conventional OAM lies in the beam propagation direction (as illustrated in Fig. 1), PSOAM antennas are specifically designed to generate transverse beams while retaining the phase characteristics of OAM. Therefore, efficient design methodologies for converting OAM beams into PSOAM beams are critical. The array elements are uniformly distributed along the circumference of a circle, and the angular spacing between two adjacent elements, measured at the circle's center, is given by the relation  $\Delta\phi = 2\pi/N$ , where  $N$  is the total number of array elements. During excitation, the phase of each array element

is adjusted based on the desired OAM mode, as defined by (3).

$$\Psi_n = \phi_0 + \frac{2ln\pi}{N} \quad (3)$$

In (3),  $\phi_0$  represents the initial phase, which is typically set to zero. The parameters involved in this equation are detailed as follows:

$$l = \pm 1, \pm 2, \dots \quad (4)$$

$$n = 0, 1, \dots, N-1$$

The number of distinguishable orbital angular momentum (OAM) modes that can be generated by a circular array is fundamentally limited by the number of its elements, as expressed in (5).

$$-\frac{N}{2} < l < \frac{N}{2} \quad (5)$$

The electric and magnetic field components of the PSOAM wave are described by (6), as presented in [17].

$$E_\phi \approx \frac{C}{\omega\epsilon} \times \frac{k^2}{r} \times e^{-jkr} e^{jl\phi} J'_l(ka) \quad (6.a)$$

$$H_z \approx C \times \frac{k}{r} \times e^{-jkr} e^{jl\phi} J'_l(ka) \quad (6.b)$$

Here,  $E$ ,  $H$ , and  $C$  represent the electric field, magnetic field, and the speed of light in free space, respectively. As expressed in (6), the phase of the electromagnetic fields in PSOAM antennas depends not only on the propagation direction but also on the rotational angle around the axis of propagation. Moreover, unlike conventional OAM antennas—where the Poynting vector exhibits a rotational behavior—the Poynting vector in PSOAM antennas is non-rotational. A more detailed theoretical explanation can be found in [13].

As an illustrative example, a circular array composed of non-metamaterial elements was simulated. Specifically, an array of eight strip-type Yagi-Uda antennas was modeled. The design specifications and dimensions of the individual elements are thoroughly described in [13]. The simulated array configuration and its corresponding radiation pattern are shown in Fig. 3.

An image of this array, along with its corresponding phase pattern, is presented in Fig. 4. The radius of the 8-element strip-type Yagi-Uda array is 36.5 mm, and the inter-element spacing can be readily calculated by multiplying the angular separation between elements (in radians) by the array radius. Based on this calculation, the inter-element distance is approximately 28.67 mm. For configurations with 9 and 10 elements, the array radius was adjusted accordingly to maintain a constant inter-element spacing.

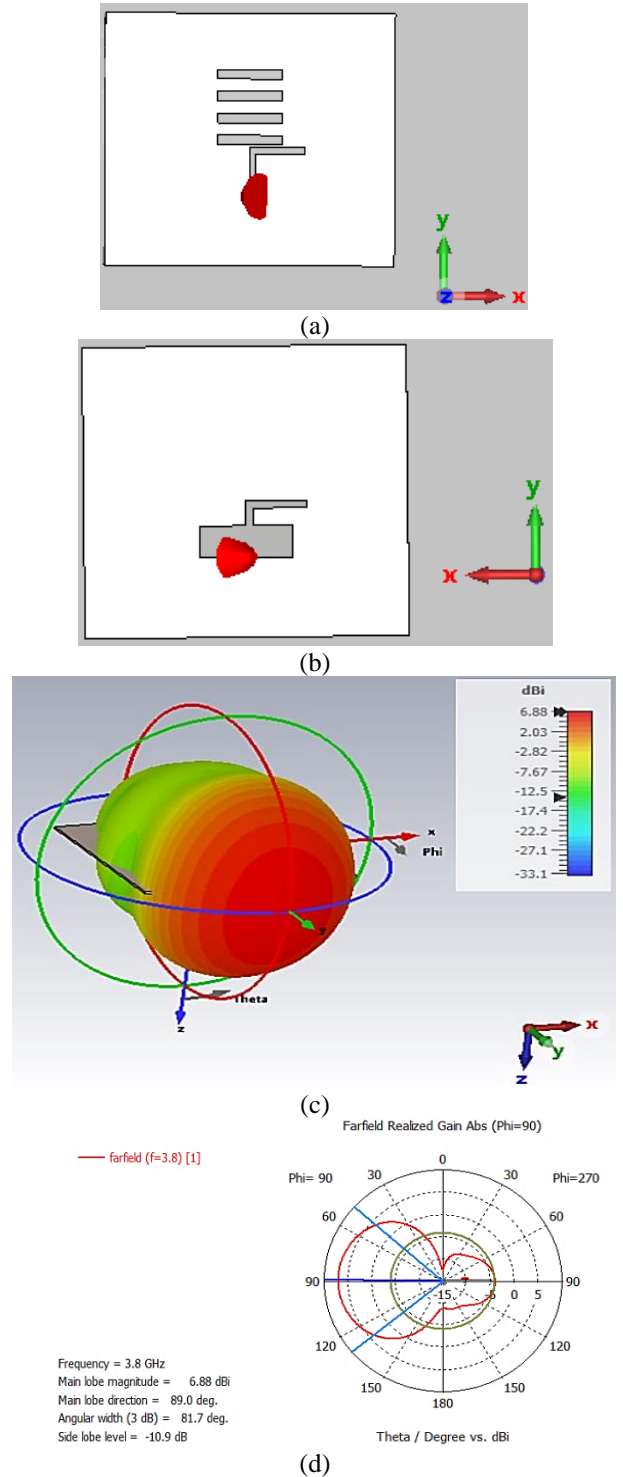


Fig. 3. Single unit cell of the Yagi-Uda microstrip array antenna: a) Top view. b) Rear view of the antenna. c) Three-dimensional radiation pattern of the array cell at 3.8 GHz. d) Two-dimensional polar radiation pattern of the array cell at the same frequency

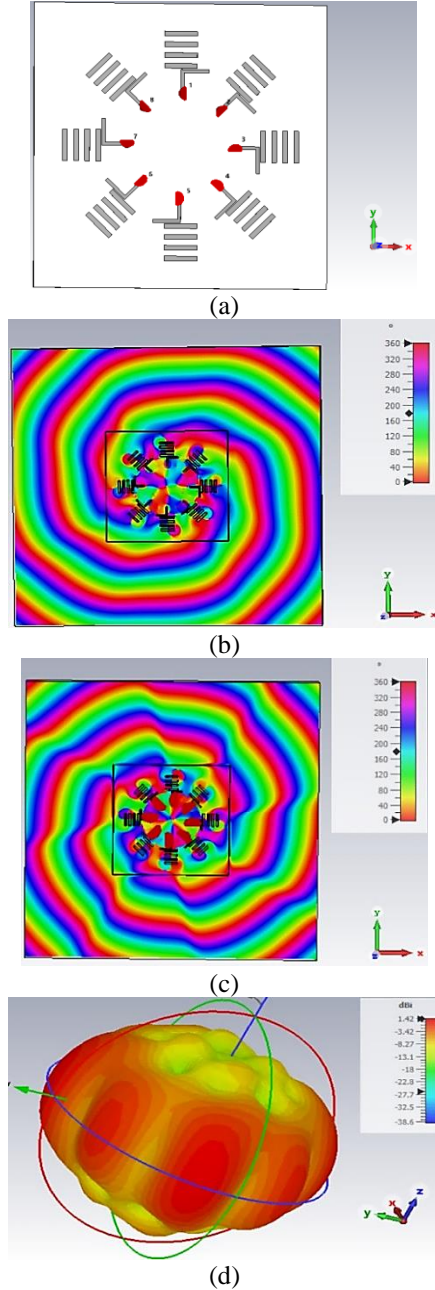


Fig. 4. Analysis of the existing 8-element microstrip Yagi-Uda array design from: a) Simulated view of the 8-element array antenna. b) Phase pattern of the array comprising 8 Yagi-Uda elements in mode +3 according to (2). c) Phase pattern of this array in mode -3. d) Three-dimensional radiation pattern

Subsequently, a circular array composed of metamaterial-based elements is investigated and simulated. The analysis of simulation results reveals that the theoretical relationships established earlier apply exclusively to conventional (non-metamaterial) circular arrays. In contrast, when metamaterial elements are employed, the relationship between the number of array elements and the achievable OAM modes no longer adheres to those conventional equations. This unique characteristic enables the generation of higher-order modes by merely adjusting the phase configuration of the elements—without the need to increase their quantity.

### III. PSOAM WAVE GENERATION USING CRLH METAMATERIAL-BASED ARRAYS

For the proposed design, a strip-type antenna based on composite right/left-handed (CRLH) metamaterials was utilized as the unit cell of the array. This choice was driven by the antenna's compact size compared to conventional strip antennas, as well as its predominantly horizontal radiation pattern. In contrast, traditional strip patch antennas typically exhibit peak radiation in a direction normal to the antenna plane. Notably, the selected unit cell achieves a relative bandwidth of 1.93%, which is considered significant for strip-type antenna designs. The simulated configuration of this antenna is shown in Fig. 5. The proposed antenna was fabricated on a Rogers 4730 substrate with a thickness of 1.52 mm, and additional design dimensions are provided in [14]. The etched patterns on the radiating patch (Fig. 5(a)) are responsible for inducing negative permittivity, while the metallic grid on the ground plane (Fig. 5(b)) contributes to negative permeability. Together, these features constitute the metamaterial structure [16].

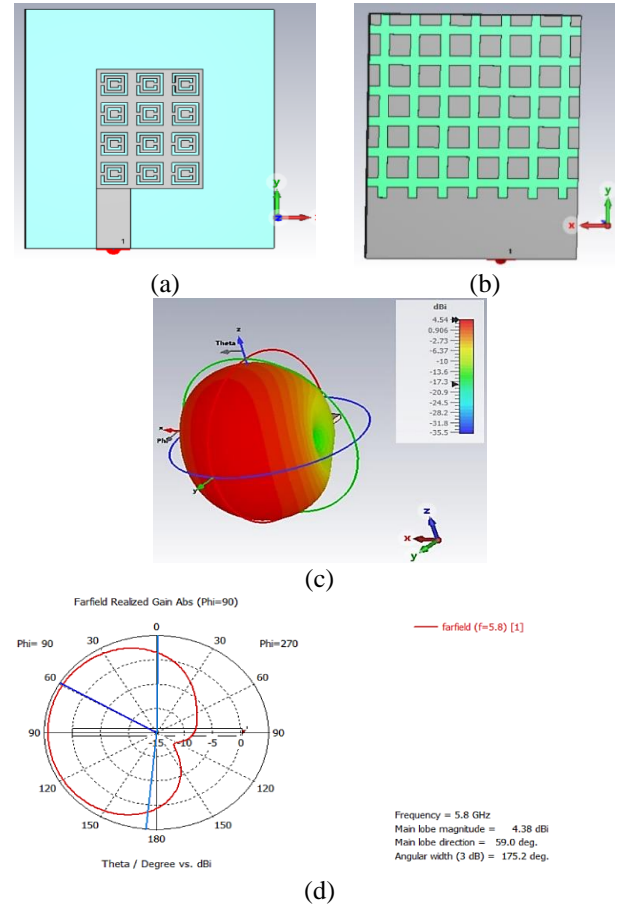


Fig. 5. Single unit cell of the proposed metamaterial array antenna: a) Top view. b) Rear view of the metamaterial-based antenna. c) Three-dimensional radiation pattern of the array cell at 5.8 GHz. d) Two-dimensional polar radiation pattern of the array cell at the same frequency

Fig. 6 shows the simulated reflection coefficient ( $S_{11}$ ) of the unit cell. As illustrated, the antenna achieves a wide impedance bandwidth, exceeding 3 GHz, centered around 5.8 GHz.

Subsequently, similar to the Yagi-Uda element-based circular array, a circular array comprising eight metamaterial elements was simulated. To generate mode -3, eight unit cells were arranged in the array according to (5). The radius of the 8-element array was set to 39 mm for the optimized configuration. Uniform excitation amplitude was applied



across all elements, while phase variations were computed using (3) to produce mode -3, following the same methodology as for the Yagi-Uda array. The proposed array configuration is depicted in Fig. 7. Following a simulation in CST Microwave Studio, the three-dimensional radiation pattern shown in Fig. 8 was obtained.

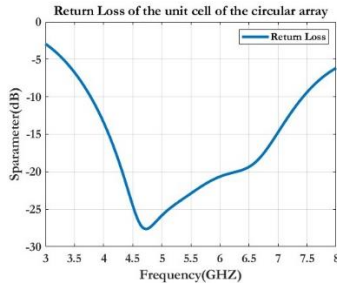


Fig. 6. Return loss plot of the single unit cell of the circular array

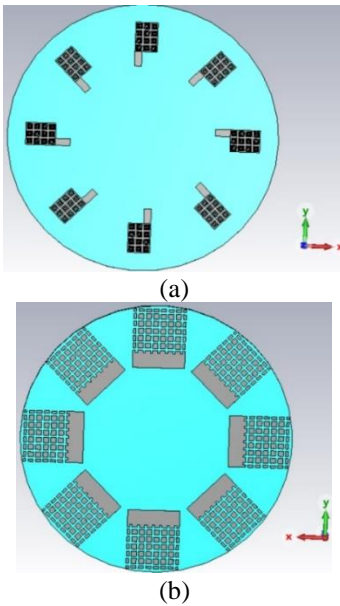


Fig. 7. Proposed array antenna for generating PSOAM: a) Top view. b) Bottom view

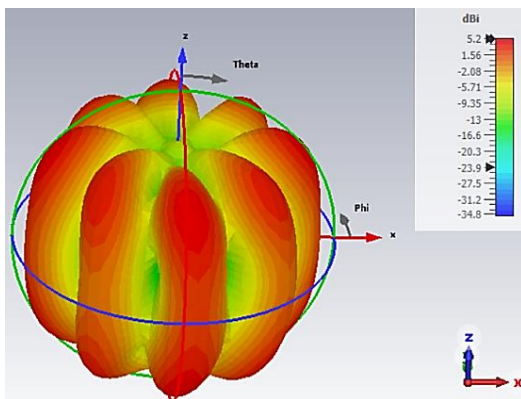


Fig. 8. Three-dimensional radiation pattern of the circular array antenna based on eight metamaterial elements at 5.8 GHz

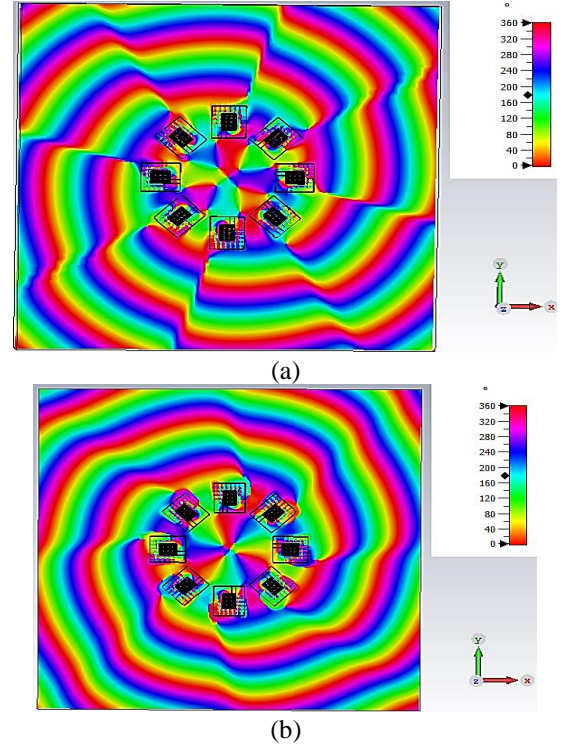


Fig. 9. Phase pattern of the circular array with eight metamaterial elements: a) Mode +3. b) Mode -3

#### IV. ANALYSIS OF METAMATERIAL ELEMENT UTILIZATION FOR HIGHER-ORDER OAM MODE GENERATION

To date, we have demonstrated that the proposed circular array design utilizing metamaterial elements challenges the conventional theory—established in references such as [13] and [18]—which posits a proportional relationship between the number of producible OAM modes and the number of array elements in circular arrays. For further analysis, both the strip-type Yagi-Uda circular array [13] and the proposed metamaterial array were simulated for various OAM modes. Simulations were performed for -9 and -10 element configurations of both metamaterial and Yagi-Uda arrays, using phase configurations derived from (3). The array radii for the 9- and 10-element Yagi-Uda arrays were set to 43.7 mm and 50.8 mm, respectively, while the corresponding metamaterial arrays had radii of 43.9 mm and 48.8 mm. The simulation results are summarized in Table I.

As shown in Table I, the electric field phase of the wave on the antenna plane depends on the rotational angle relative to the array axis, consistent with (6). The color spectrum represents phase variations ranging from 0 to 360 degrees, where the number of repeating color cycles corresponds to the OAM mode order. Clockwise and counterclockwise rotations indicate positive and negative mode indices, respectively. Notably, Table I reveals that the phase patterns produced by the metamaterial array do not consistently conform to (5), demonstrating unprecedented behavior.

For a detailed analysis of the anomalous phase patterns observed in the metamaterial array, Table II is provided. Here, "anomalous behavior" refers to phase patterns that exceed the theoretical limits established by (5). This behavior arises in metamaterial arrays when excited with phase configurations corresponding to mode +2 and persists for higher-order modes. A consistent anomaly observed across all cases is the generation of negative mode phase patterns despite excitation with positive mode indices. For example, as shown in Table II, when 8-, 9-, and 10-element arrays are

excited with phase configurations for OAM modes +2, +3, and +4, the resulting phase patterns correspond to modes -5, -6, -7, and -8. Since these patterns contradict (5), the use of metamaterials in PSOAM antennas introduces a novel characteristic.

In contrast to reference 15, where no reduction in the number of metamaterial-based circular array elements was

achieved and the generated phase pattern remained consistent with conventional theory, this paper demonstrated that, contrary to conventional theory, a PSOAM antenna with a different phase pattern can be designed by using electromagnetic metamaterial. Meanwhile, [15] also exhibits a narrower bandwidth compared to the results of this study.

TABLE I

Comparison of the Generated Phase Patterns for Different Phase Excitations Between the Proposed Metamaterial Design and the Microstrip Yagi-Uda Array Design with 9 and 10 Elements

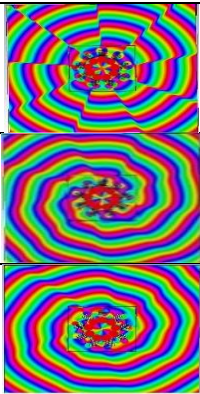

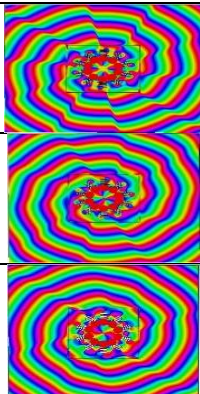

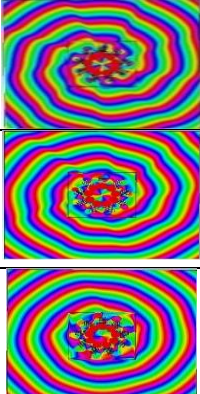
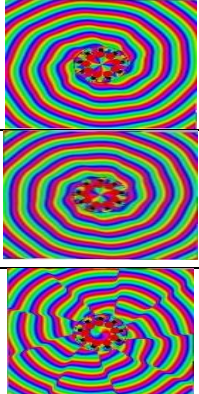
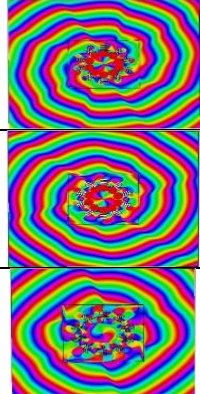
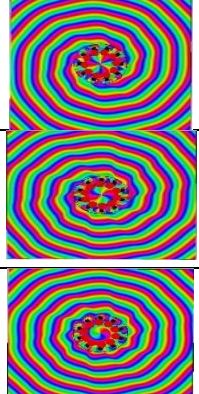
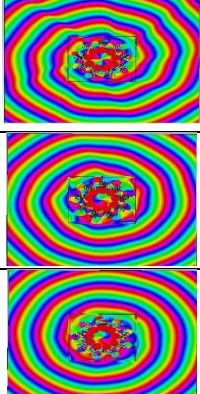
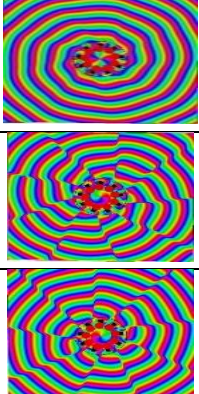
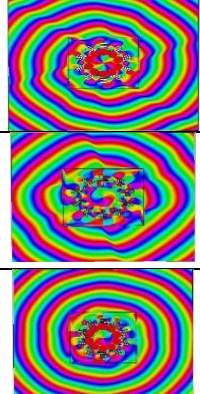
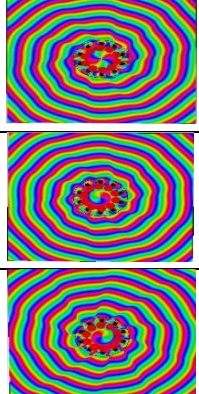
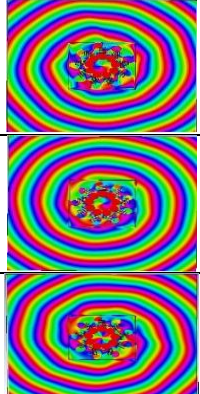
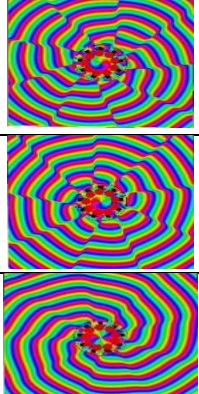
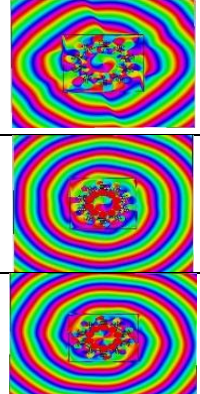
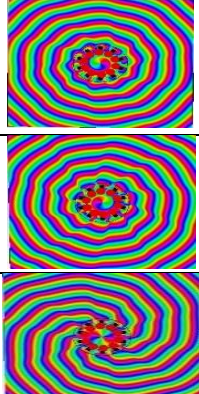
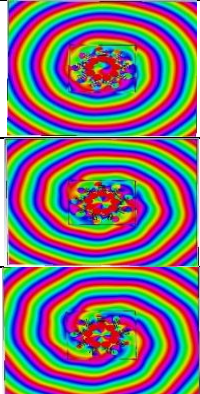
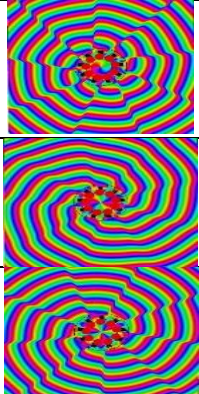
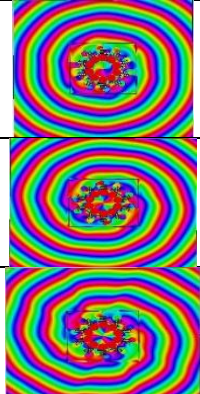

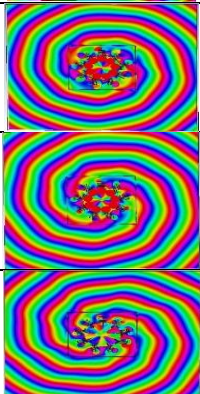

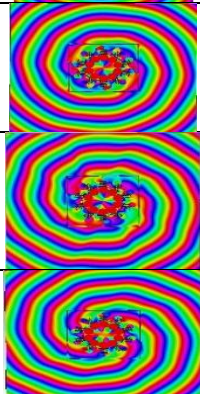

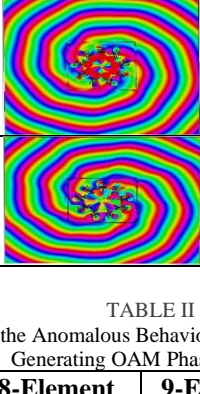

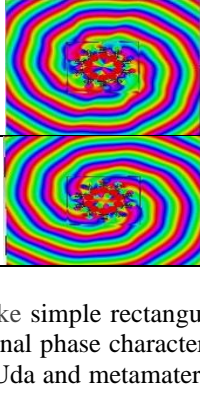
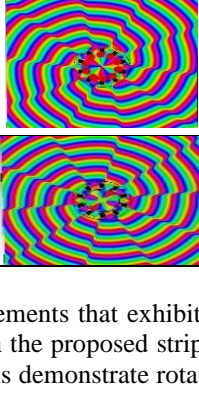
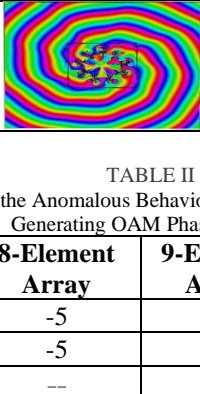
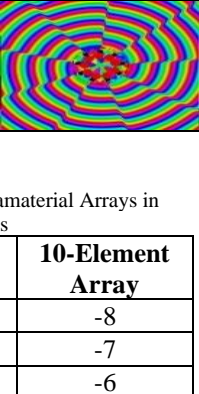
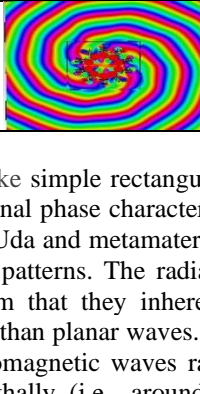
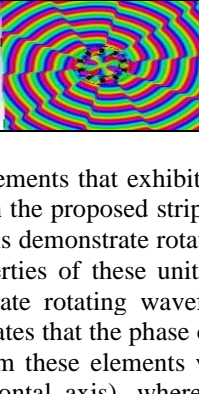
Feeding Mode	Yagi-Uda 9-Element Antenna	9-Element Metamaterials	10-Element Yagi-Uda Antenna	10-Element Metamaterials
Mode -4				
Mode -3				
Mode -2				
Mode -1				
Mode 1				
Mode 2				
Mode 3				
Mode 4				

TABLE II

Investigation of the Anomalous Behavior of Metamaterial Arrays in Generating OAM Phase Patterns

	8-Element Array	9-Element Array	10-Element Array
Mode 2	-5	-7	-8
Mode 3	-5	-6	-7
Mode 4	---	-5	-6

To investigate this phenomenon further, the phase patterns of individual elements within the arrays were analyzed, with the results shown in Fig. 10. Notably, Figs. 10(b) and 10(c) illustrate that both the strip-type Yagi-Uda and metamaterial unit cells exhibit rotational phase patterns. In contrast, the rectangular strip element depicted in Fig.10(a) shows no rotational phase pattern, instead producing a planar wave.

Unlike simple rectangular strip elements that exhibit non-rotational phase characteristics, both the proposed strip-type Yagi-Uda and metamaterial unit cells demonstrate rotational phase patterns. The radiation properties of these unit cells confirm that they inherently generate rotating wavefronts rather than planar waves. This indicates that the phase of the electromagnetic waves radiated from these elements varies azimuthally (i.e., around the horizontal axis), whereas in planar waves, phase variation depends solely on the radial distance from the source.

However, previous studies [13], [19] have demonstrated that both conventional strip and Yagi-Uda elements adhere to the phase pattern relationship described by (5). Therefore, the rotational or non-rotational nature of the phase pattern of individual elements cannot account for the deviation observed in the metamaterial array's modal-element



relationship. We thus conclude that the metamaterial composition of the array elements is the primary factor responsible for the anomalous OAM phase patterns observed.

As indicated by (6), unlike conventional planar waves, the phases of the electric and magnetic fields in PSOAM antennas depend on the rotational angle around the axis perpendicular to the antenna plane. Accordingly, as illustrated in Fig. 10, both the metamaterial and Yagi-Uda array unit cells generate PSOAM waves, with their electric field phases varying azimuthally with respect to rotation about this axis (Figs. 10(b) and 10(c)). In contrast, conventional patch antennas show no such dependence, as their phase variation is solely a function of the radial distance from the antenna.

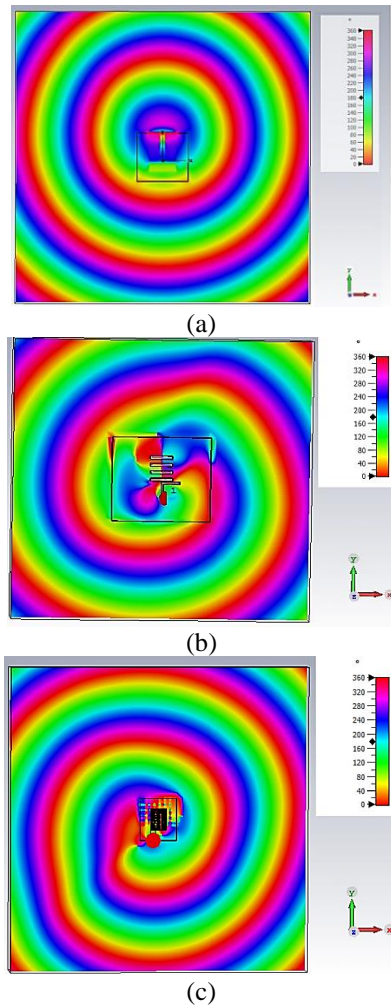


Fig. 10. a) Phase pattern of a simple microstrip antenna cell. b) Phase pattern of the microstrip Yagi-Uda antenna cell used in the array shown in Fig. 4. c) Phase pattern of the metamaterial unit cell in the proposed array design shown in Fig. 7

Figs. 10(b) and 10(c) show that if the anomalous phase patterns observed in the metamaterial circular array were solely due to the rotational phase characteristics of its unit cells, a similar behavior would be expected in the Yagi-Uda array, whose unit cells also exhibit rotational phase patterns. However, the Yagi-Uda PSOAM array conforms to (5), demonstrating conventional behavior. Therefore, we attribute the anomalous phase patterns exclusively to the metamaterial properties.

It is worth noting that detailed phase pattern analyses were performed not only on the three antenna types shown in Fig. 10 but also on other antennas, such as horn antennas and non-

printed Yagi designs. These phase patterns were examined across multiple cross-sectional planes of their 3D radiation profiles. However, since a comprehensive discussion exceeds the scope of this paper, we focus here solely on the results presented in Fig. 10.

Since, as illustrated in Fig. 5(d), the direction of maximum radiation of the metamaterial array unit cell is not aligned with the horizontal axis but rather tilted, a corner reflector was added behind it, and the resulting phase pattern was investigated. The observed phase pattern was consistent with the results reported in the referenced article. For the sake of brevity, and given that the primary objective was to highlight the anomalous phase pattern arising from the use of metamaterials, the diagrams and results corresponding to the case with the added reflector have been omitted.

## V. CONCLUSION

This paper has demonstrated the generation of plane spiral orbital angular momentum (PSOAM) waves using a strip-type array antenna composed of metamaterial-based unit cells. To the best of our knowledge, this work represents the first study to utilize electromagnetic metamaterials for realizing antennas with vortex phase fronts. Simulations conducted in CST Microwave Studio conclusively show that metamaterials facilitate the generation of higher-order OAM modes with fewer array elements than conventional circular arrays and previously established theoretical limits. Moreover, we have shown that the rotational or non-rotational phase behavior of individual elements does not explain the metamaterial array's deviation from the traditional modal-element relationship described in (5). Instead, the observed anomalous phase patterns are exclusively attributable to the unique electromagnetic properties of the metamaterial elements employed.

## REFERENCES

- [1] J. H. Poynting, "The wave motion of a revolving shaft, and a suggestion as to the angular momentum in a beam of circularly polarised light," *Proc. R. Soc. Lond. A*, vol. 82, no. 557, pp. 560–567, 1909. DOI: <https://doi.org/10.1098/rspa.1909.0060>.
- [2] R. A. Beth, "Mechanical detection and measurement of the angular momentum of light," *Phys. Rev.*, vol. 50, no. 2, pp. 115–125, 1936. DOI: <https://doi.org/10.1103/PhysRev.50.115>.
- [3] L. Allen, M. W. Beijersbergen, R. J. Spreeuw, and J. P. Woerdman, "Orbital angular momentum of light and the transformation of Laguerre-Gaussian laser modes," *Phys. Rev. A*, vol. 45, no. 11, pp. 8185–8189, 1992. DOI: [10.1103/PhysRevA.45.8185](https://doi.org/10.1103/PhysRevA.45.8185).
- [4] G. A. Turnbull, D. A. Robertson, G. M. Smith, L. Allen, and M. J. Padgett, "The generation of free-space Laguerre-Gaussian modes at millimetre-wave frequencies by use of a spiral phase plate," *Opt. Commun.*, vol. 127, no. 4, pp. 183–188, 1996. DOI: [10.1016/0030-4018\(96\)00070-3](https://doi.org/10.1016/0030-4018(96)00070-3).
- [5] Q. Bai, A. Tennant, and B. Allen, "Experimental circular phased array for generating OAM radio beams," *Electron. Lett.*, vol. 50, no. 20, pp. 1414–1415, 2014. DOI: [10.1049/el.2014.2860](https://doi.org/10.1049/el.2014.2860).
- [6] Y. Cheng, X. Zhou, X. Xu, Y. Qin, and H. Wang, "Radar coincidence imaging with stochastic frequency modulated array," *IEEE J. Sel. Topics Signal Process.*, vol. 11, no. 2, pp. 414–427, Mar. 2017. DOI: [10.1109/JSTSP.2016.2615275](https://doi.org/10.1109/JSTSP.2016.2615275).
- [7] K. Liu, Y. Cheng, X. Li, and Y. Gao, "Microwave-sensing technology using orbital angular momentum: Overview of its advantages," *IEEE Veh. Technol. Mag.*, vol. 14, no. 2, pp. 112–118, Jun. 2019. DOI: [10.1109/MVT.2018.2890673](https://doi.org/10.1109/MVT.2018.2890673).
- [8] T. Yuan, H. Wang, Y. Qin, and Y. Cheng, "Electromagnetic vortex imaging using uniform concentric circular arrays," *IEEE Antennas Wireless*

Propag. Lett., vol. 15, pp. 1024–1027, 2016. DOI: 10.1109/LAWP.2015.2490169.

[9] M. Zhao, X. Gao, M. Xie, W. Zhai, W. Xu, S. Huang, and W. Gu, "Measurement of the rotational Doppler frequency shift of a spinning object using a radio frequency orbital angular momentum beam," Opt. Lett., vol. 41, no. 11, p. 2549, May 2016. DOI: 10.1364/OL.41.002549.

[10] A. Vaziri, G. Weihs, and A. Zeilinger, "Superpositions of the orbital angular momentum for applications in quantum experiments," J. Opt. B, Quantum Semiclass. Opt., vol. 4, no. 2, pp. S47–S51, Mar. 2002. DOI: 10.1088/1464-4266/4/2/367.

[11] L. Xiaoyu, Z. Yongzhong, and P. Guohao, "A Microstrip Yagi Antenna Array Generating Plane Spiral Orbital Angular Momentum Wave," 2020 International Conference on Microwave and Millimeter Wave Technology (ICMMT), Shanghai, China, pp. 1-3, 2020. DOI: 10.1109/ICMMT49418.2020.9386564.

[12] Z. Zhang, S. Zheng, X. Jin, H. Chi, and X. Zhang, "Generation of Plane Spiral OAM Waves Using Traveling-Wave Circular Slot Antenna," in IEEE Antennas and Wireless Propagation Letters, vol. 16, pp. 8-11, 2015. DOI: 10.1109/LAWP.2016.2552227.

[13] X. Y. Liu, Y. Zhu, W. Xie, G. H. Peng, and W. Wang, "Generation of Plane Spiral Orbital Angular Momentum Waves by Microstrip Yagi Antenna Array," in IEEE Access, vol. 8, pp. 175688-175696, 2020. DOI: 10.1109/ACCESS.2020.3026241.

[14] Hasan Onder Yilmaz, Fatih Yaman "Meta-material Antenna Designs for a 5.8 GHz Doppler Radar," in IEEE Transactions on Instrumentation and Measurement, vol. 69, pp. 1775-1782, 2020. DOI:10.1109/TIM.2019.2914131.

[15] Amir Habibi Daronkola, Farzad Tavakol Hamedani, Pejman Rezaei, "Design and Implementation of a New Method for Producing Transverse OAM with Metamaterial Antenna Structure", Arabian Journal for Science and Engineering, 50:5853–5868, 2024, DOI: 10.1007/s13369-024-09659-2

[16] M. Danaeian, H. Ghayoumizadeh, "A Compact Narrow Band-Pass Filter Based on Composite Right-Left Handed Structures for WLAN Application," Journal of Applied Electromagnetics, Vol. 7, No.1, 2019.

[17] S. Zheng, Z. Zhang, Y. Pan, X. Jin, H. Chi, and X. Zhang, "Plane spiral orbital angular momentum electromagnetic wave," 2015 Asia-Pacific Microwave Conference (APMC), Nanjing, China, 2015, pp. 1-3, doi: 10.1109/APMC.2015.7413418.

[18] Yongzhong Zhu, Weiguo Dang, Xiaoyu Liu, Yijun Chen, Xiaofei Zhou & Hongyan Lu "Generation of plane spiral orbital angular momentum using circular double-slot Vivaldi antenna array," Scientific Reports, vol. 10, no. 1, p.18328, 2020. DOI: 10.1038/s41598-020-75202-6.

[19] Q. Ma, S. Zheng, J. Zheng, Y. Chen and X. Zhang, "Realization of Structured Electromagnetic Waves Based on Plane Spiral Orbital Angular Momentum Waves Using Circular Cylindrical Conformal Microstrip Antenna Array," 2018 Asia-Pacific Microwave Conference (APMC), Kyoto, Japan, pp. 91-93, 2018. DOI: 10.23919/APMC.2018.8617400.